American Mineralogist, Volume 76, pages 1467–1478, 1991

Microstructures and fiber-formation mechanisms of crocidolite asbestos

JUNG HO AHN,* PETER R. BUSECK
Departments of Geology and Chemistry, Arizona State University, Tempe, Arizona 85287-1404, U.S.A.

ABSTRACT

Asbestiform riebeckite (crocidolite) from the Marra Mamba Iron Formation (Hamersley Basin, Western Australia) was investigated using high-resolution transmission electron microscopy (HRTEM). Crocidolite asbestos consists of bundles of fibers 0.03 to 0.5 μm in diameter that are slightly rotated with respect to each other. The fibers contain wide-chain pyriboles and sparse single-chain structures. The only sheet silicate intergrown with crocidolite has a mica structure; the Fe- and Na-rich composition of crocidolite presumably accounts for the absence of serpentine and chlorite.

Some fibrous crystals are polygonized to subgrains that are slightly rotated relative to one another; individual subgrains are connected by coherent wide-chain pyriboles at (010) interfaces. Many fibrous crystals contain (110) and (100) planar defects across which crystal misorientation occurs; such areas commonly contain Burgers vectors parallel to **a***, implying that edge dislocation components are associated with these planar defects. The dislocations seem to have formed during initial crystallization, and they apparently serve as "seeds" for planar defects that eventually developed into subgrain boundaries. Imposition of tectonic stresses on defect-rich and polygonized crystals would favor the further development of fibers by separating crystals along a variety of defects and subgrain boundaries. The abundant planar defects that are extended along the fiber axes enhance the tensile strength of crocidolite fibers by mitigating the propagation of cracks and by providing sites for interplanar slip.

INTRODUCTION

There are four main varieties of asbestiform amphibole: crocidolite (a fibrous variety of riebeckite), amosite (a fibrous variety of grunerite), anthophyllite, and tremolite-actinolite. These minerals can occur in commercial quantities and have been mined because of their valuable physical properties. Asbestiform amphiboles easily separate into elongated fibers, each of which is extremely strong and flexible. Amphibole asbestos is a well-known health hazard, and it is of much current interest because of its relation to environmental health problems (e.g., Ross, 1981; Skinner et al., 1988; Mossman et al., 1990a, 1990b).

The chain structure of amphibole and its various defect structures are thought to account for the occurrence of its fibrous varieties (Chisholm, 1973; Hutchison et al., 1975), but the exact causes of the differences in physical properties between asbestiform and massive amphiboles are still unresolved. Many transmission electron microscopy (TEM) studies have been performed to investigate structural defects that may be important for controlling the crystal habits and physical properties of amphibole asbestos. Chisholm (1973) and Hutchison et al. (1975) showed the presence of (100) twins and Wadsley defects on (010) and (110) of various fibrous amphiboles. Veblen et al. (1977) suggested that asbestiform anthophyllite selectively breaks along (100) twin planes or stacking faults and also along chain-width defects. Veblen (1980) suggested breakage along the (010) wide-chain pyriboles, (100) faults, and the grain boundaries between individual crystallites as the primary mechanisms of fiber formation. Whittaker et al. (1981) and Cressey et al. (1982) observed that amosite also contains various chain-width defects and termination defects that are similar to those reported by Veblen and Buseck (1980) for anthophyllite.

Crocidolite asbestos, which has the greatest tensile strength among the asbestos fibers, is prominent in banded iron formations in the Transvaal Supergroup, South Africa (e.g., Cilliers and Genis, 1964) and in the Hamersley Basin, Western Australia (e.g., Trendall and Blockley, 1970). Using TEM, Alario Franco et al. (1977) showed cross sections of crocidolite fibers and found they contain intergrown wide-chain structures. Crawford (1980) observed various planar defects and surface-dissolution features in crocidolite fibers.

The present study is an investigation of the structural defects and grain-boundary structures of crocidolite and their relation to the origin of its fibrous habit and high tensile strength. Although most defect structures observed in crocidolite are similar to those in anthophyllite and other biopyriboles described by Veblen and Buseck (1980), some of the defects observed in the present study

* Present address: Korea Ocean Research and Development Institute, Ansan P.O. Box 29, Ansan, Seoul, Korea.

0003–004X/91/0910–1467$02.00

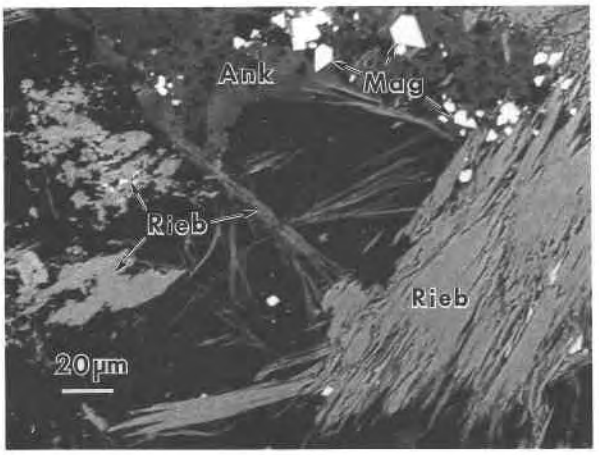

Fig. 1. Backscattered electron (BSE) image of the Marra Mamba specimen. Most riebeckite (Rieb) occurs as bundles of fibers. Ankerite (Ank) does not show well-defined crystal shapes, but magnetite (Mag) occurs as euhedral crystals.

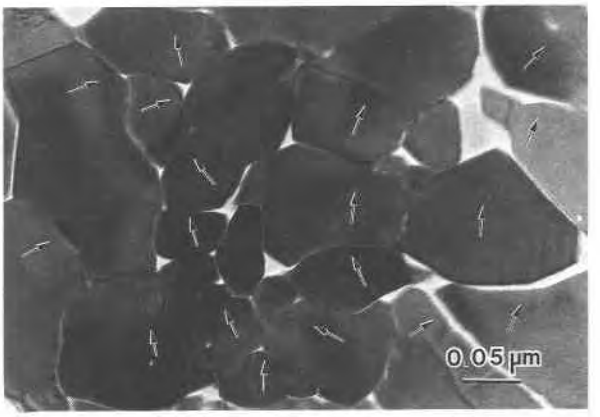

Fig. 2. Low-magnification image of crocidolite along [001], showing the cross sections of fibrous crystals. Many cross sections are irregular in outline. The arrows indicate the **a*** direction, which was determined from the orientation of intergrown wide-chain slabs.

differ. We also investigated intergrowths of wide-chain pyriboles and sheet silicate because such intergrowths can result in significant changes in physical properties and compositions.

Specimens and electron-microscope analyses

We studied samples from a drill hole (DDH no. 270) in the Marra Mamba Iron Formation, Hamersley Basin, Western Australia, located 38 km west of Wittenoom. The specimens were collected from the upper 2 m of the Mount Newman Member. Petrologic study of closely associated, underlying volcanics indicated a range of burial metamorphic conditions within the prehnite-pumpellyite facies (Klein and Gole, 1981). The mineralogy and petrology of samples from this drill hole were described by Ewers and Morris (1980) and Klein and Gole (1981).

The crocidolite crystals in our specimens occur as bundles of fibers and as sprays of fibrous crystals (Fig. 1). Electron microprobe analyses are listed in Table 1. Although an electron beam with a 2-μm diameter was used for the analyses, TEM observation indicates that it is almost impossible to exclude the wide-chain pyriboles and micas that are intergrown with the crocidolite.

Table 1. Representative electron microprobe analyses of three crocidolite crystals

	1	2	3
SiO_2	52.59	52.17	52.24
Al_2O_3	0.03	0.02	0.03
FeO	32.27	33.05	33.12
MgO	4.77	4.43	4.22
MnO	0.02	0.00	0.00
TiO_2	0.00	0.00	0.00
K_2O	0.04	0.03	0.06
Na_2O	6.94	7.01	7.15
CaO	0.39	0.29	0.43
Total	97.05 wt%	97.00 wt%	97.25 wt%
Si	7.997	7.997	7.995
$^{[4]}Al$	0.003	0.003	0.005
Sum	8.000	8.000	8.000
$^{[6]}Al$	0.003	0.000	0.000
Fe^{2+}	2.665	2.916	2.910
Fe^{3+}	1.438	1.321	1.329
Mg	1.081	1.012	0.963
Mn	0.003	0.000	0.000
Ti	0.000	0.000	0.000
Ca	0.064	0.048	0.071
Na	1.746	1.703	1.727
Sum	7.000	7.000	7.000
Na	0.300	0.380	0.394
K 0.008	0.006	0.012	
Sum	0.308	0.386	0.406
Total	15.308	15.386	15.406
Fe/(Fe + Mg)	79.15%	80.72%	81.49%

Note: 1: The unit-cell contents are calculated based on a formula unit having 23 O atoms. 2: The Fe^{2+}/Fe^{3+} ratio was determined by the method of Papike et al. (1974). 3: The analysis totals are low because of the presence of OH in the amphibole structure.

Experimental

Ion-milled specimens were prepared from petrographic thin sections following the procedure described by Ahn et al. (1988). Specimens were examined at 400 kV with a JEOL JEM-4000EX transmission electron microscope that has a top-entry, double-tilting sample holder ($\pm 15°$ tilt). The microscope has a structure resolution limit of 1.7 Å and a spherical aberration coefficient (C_S) of 1.0 mm. The features and performance of the microscope were described by Smith et al. (1986). A 40-μm objective aperture and a 150-μm condenser aperture were used for high-resolution transmission electron microscopy (HRTEM) imaging. Analytical electron microscopy (AEM) was performed using a Philips 400T 120-kV transmission electron microscope with an attached Tracor Northern TN-2000 multichannel analyzer for energy-dispersive X-ray analysis.

Images of amphibole and wide-chain pyriboles were interpreted in accordance with the image simulations of Veblen and Buseck (1979a), who showed that the positions of the I-beam units of amphiboles correspond to the dark areas for a wide range of underfocus conditions.

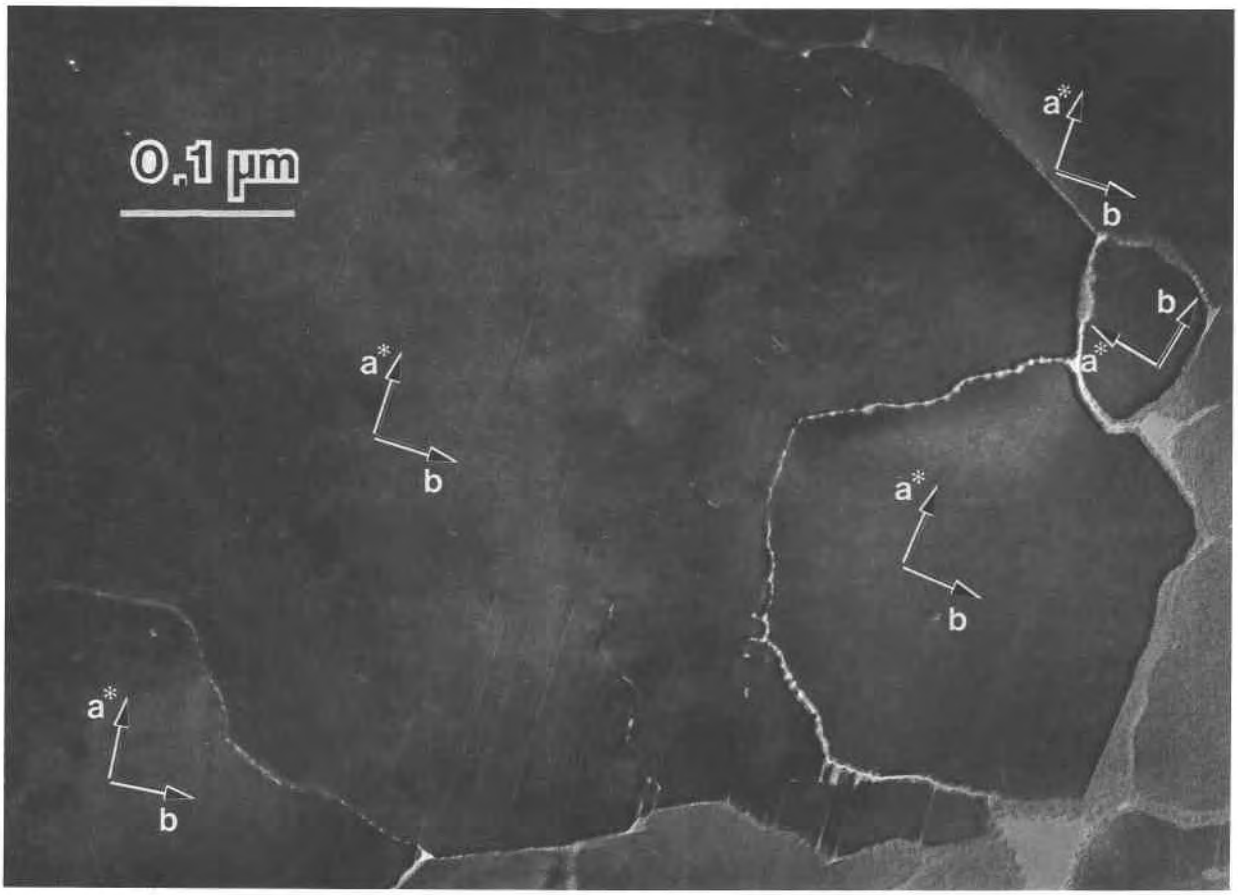

Fig. 3. Low-magnification image of a relatively large crocidolite crystal, the edge of which shows the development of smaller crystals having similar orientations. The small crystals have irregular grain boundaries. The large crystal contains abundant defects that result in white contrast in the image.

TEM RESULTS

Cross sections of fibers

Crocidolite fibers are elongated along **c***, and so [001] TEM images show the shapes and dimensions of the fiber cross sections. Linear features, evident in low-magnification images, indicate intergrowths of wide-chain pyriboles (Fig. 2). Such features are useful for determining the **a*** direction in low-magnification TEM images in which the white spots between I-beams are not resolved (Veblen and Buseck, 1980).

We observed textural features similar to those described by Alario Franco et al. (1977). Crocidolite fibers exhibit a range of widths, but most have diameters less than 0.1 μm (Fig. 2). Although many cross sections exhibit irregular edges, (110) grain boundaries coincident with the cleavage planes of amphibole are common. Most individual fibers are rotated by several degrees with respect to their neighbors. Cressey et al. (1982) also observed that elongated amosite crystals grow with rotational disorder. Empty holes are common near the triple junctions of fibers (Fig. 2). The grain boundaries are ion milled preferentially, and the holes apparently form during ion milling.

In addition to the small fibers, crystals with cross sections as large as 1 μm occur (Fig. 3). Most have irregular outlines. Small irregular crystals are common at the edges of such large crystals, and some of these small crystals have orientations similar to their larger neighbors.

Chain-width defects

Crocidolite contains intergrown wide-chain silicates, most of which are three, four, or five chains wide (Fig. 4). The wide-chain structures are mainly concentrated close to the grain boundaries; in some fibers, only double-chain structures occur. The intergrown (010) slabs of pyriboles were called "zippers" by Veblen and Buseck (1980). In the crocidolite, most zippers propagate from grain boundaries and terminate according to the zipper-termination rules of Veblen and Buseck (1980). A variety of defects occur where wide-chain pyriboles terminate incoherently; these are described below. Crystals containing ordered intergrowths of wide chains were not observed.

Single-chain structures occur in addition to the wide-chain silicates. Figure 5 shows a quintuple-chain slab terminating incoherently to three double chains at one end and to two double chains plus one single chain at the

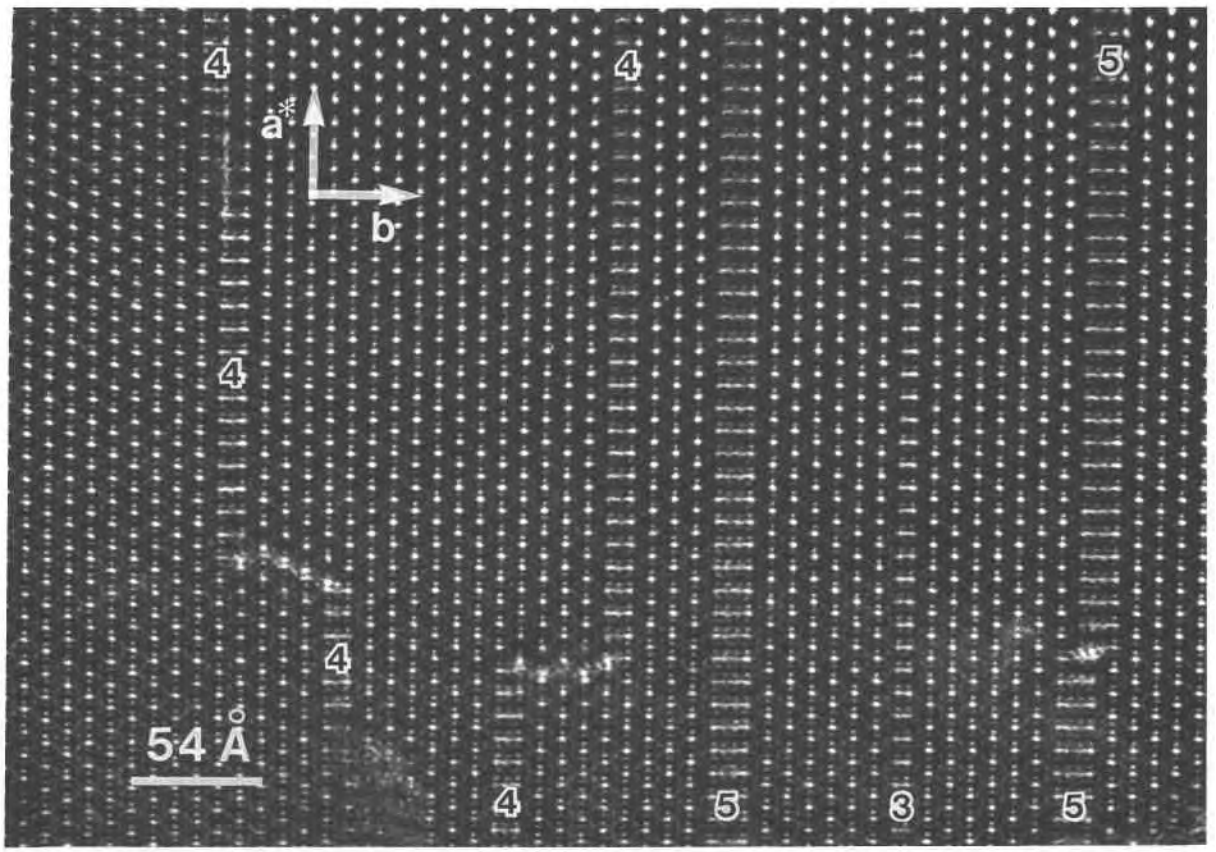

Fig. 4. HRTEM image showing intergrowths of a variety of wide-chain pyriboles. Zipper terminations are common. The integers indicate the chain-widths of the silicates.

other end. Single-chain structures are sparse, and multiple slabs of single chains were not observed. Both single- and quintuple-chain slabs result in out-of-phase boundaries between amphiboles (Veblen and Buseck, 1981). Intergrown single chains in crocidolite fibers were first reported by Crawford (1980).

Alteration to sheet silicate

Locally the amphibole has been replaced by a sheet silicate having a mica structure. Most mica occurs at the grain boundaries between fibers (Fig. 6), although in a few places it is also contained as patches within amphibole. The mica lamellae are typically approximately 100 Å thick. The small grain sizes and intimate intergrowths of mica with crocidolite precluded AEM analysis of pure mica, but analyses of overlapping areas suggest that the minerals are similar in composition. The d_{001} value of mica is almost identical to that of crocidolite (~9.53 Å) in the same HRTEM images, suggesting that the mica is more similar to sodium biotite ($d_{001} \simeq 9.6$ Å) than to a talc-like mineral ($d_{001} \simeq 9.3$ Å).

Most intergrown micas have (010) or (110) interfaces with amphibole (Fig. 6). HRTEM images of (010) crocidolite-mica interfaces do not display any disruptions or strain features, indicating that the interface is structurally coherent (Fig. 7). Paired white spots in amphibole images correspond to the tunnels on both sides of the A sites, and the white spots of mica match those in the interlayers (e.g., Iijima and Buseck, 1978). Figure 7 indicates that the **a**-axis of mica is parallel to the **c**-axis of crocidolite. The white spots in mica show that the stacking is relatively well ordered, in contrast to the talc that is intergrown with anthophyllite and wide-chain pyriboles (Veblen and Buseck, 1979b, 1980).

The alteration features of crocidolite investigated in this study differ from those of anthophyllite, in which three different sheet silicates (talc, serpentine, and chlorite) are commonly intergrown (Veblen and Buseck, 1979b, 1980; Veblen, 1980). Only mica is intergrown with the crocidolite, suggesting that the composition of the amphibole is important for controlling the alteration. Although other elements may also be involved in determining the hydration reaction of amphiboles, the high Fe/(Fe + Mg) ratio and the presence of Na in crocidolite are mainly responsible for the absence of serpentine or chlorite as alteration products.

Structural defects

Crocidolite exhibits a variety of displacive faults, many of which resemble those that were described by Veblen and Buseck (1980). In particular, ¼[010] and ½[100] faults are common in areas where incoherent zipper termina-

tions occur (½[100] in $C2/m$ amphibole is equivalent to ¼[100] in *Pnma* amphibole). However, defects that have unusual displacements also occur in crocidolite crystals. Figure 8 shows an area where a triple-chain slab terminates incoherently to a double-chain slab, resulting in an ⅛[010] displacement, which is half that of a ¼[010] fault. A ⅛[010] fault can compensate for only half of the chain-width difference between double and triple chains. The remaining misfit is accommodated by a slight distortion of the amphibole structure on one side of the termination (Fig. 8).

Unusual displacive faults also occur along (100). Figures 9A and 9B show ¼[100] faults. In the amphibole structure, cations in M4 sites are coordinated to the basal O atoms of tetrahedral strips of adjacent I-beam units. A ¼[100] fault along (010) will disrupt such a structural arrangement and result in breaking of bonds of I-beam units across (010).

The structural defects described above result in displacements along certain crystallographic directions, so they do not produce rotations across the defects. However, slight rotations parallel or nearly parallel to the c-axes of some crystals occur across certain defects (Figs. 10, 11, and 12). In Figure 10, crystal misorientation occurs across (100) defects (area A); incoherent terminations of two triple chains result in ¼[010] displacements along (100). The (100) slip plane caused by the ¼[010] fault is unusual. Faults of ¼[010] displacement are common along (110) since such offsets produce a conformable topological arrangement of I-beam units across the slip plane (Veblen and Buseck, 1980).

A triple chain grades into a double chain in area A of Figure 11, and a slight misorientation occurs across the defect. The defect is approximately parallel to (110). Such a termination is not in accord with any of the zipper termination rules of Veblen and Buseck (1980); a slight rotation across the defect adjusts for the misfit. Wide-chain pyriboles are commonly associated with defects showing such slight misorientations. However, crystal rotation can also occur across defects that do not involve intergrowths of wide-chain slabs, as shown in area B of Figure 11. A traverse around the defect results in a projected Burgers vector of 1[100], indicating that an edge-dislocation component is present. Since a screw component of a Burgers vector parallel to [001] cannot be observed in [001] images, the presence of a screw component is indeterminate.

The (110) and (100) defects are coupled in some crocidolite crystals, and slight rotations occur across such coupled defects (Fig. 12). Incoherent termination of a triple chain results in displacement faults along both (100) and (110) in the defect area. There is a single-chain width difference across the defect.

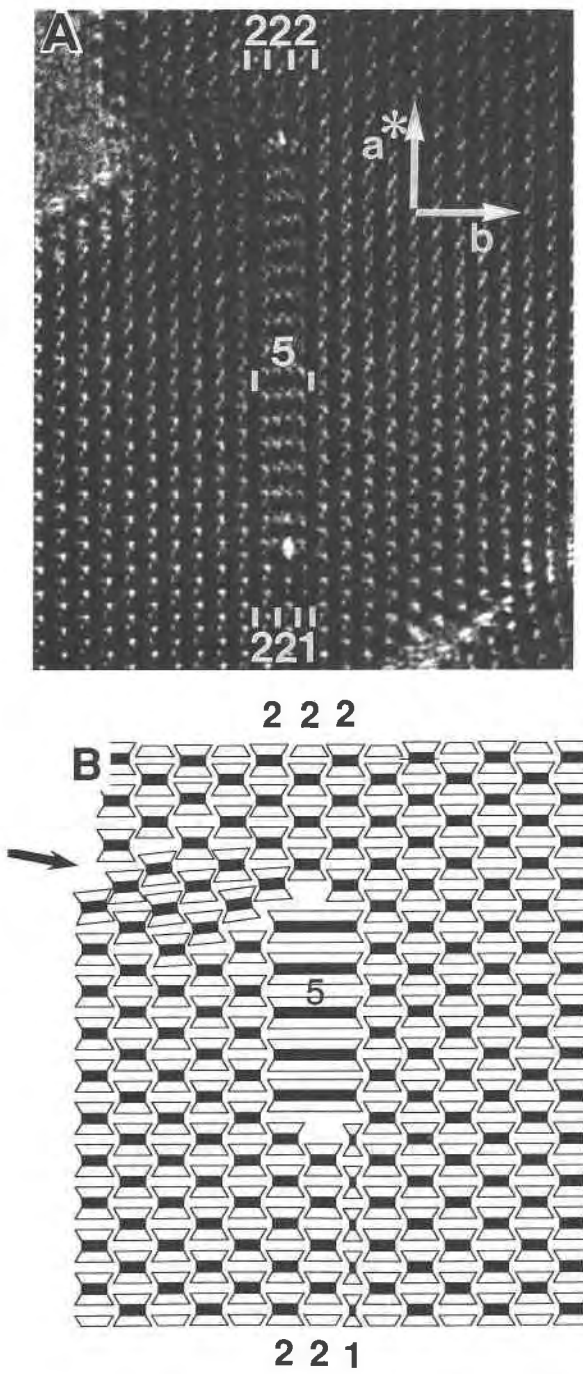

Fig. 5. (**A**) HRTEM image of an intergrowth of a single chain within crocidolite. The single chain occurs where a quintuple chain (5) terminates to two double chains plus a single chain (221). The quintuple chain also terminates incoherently to three double chains (222). (**B**) A schematic I-beam model showing the features in **A**; the arrow points to a disrupted region resulting from the structural mismatch. The termination of a quintuple-chain slab producing a single-chain slab is consistent with the out-of-phase boundary model of Veblen and Buseck (1981).

Subgrains and low-angle grain boundaries

Some large crystals are polygonized into subgrains that are misoriented by only a few degrees (Fig. 13). Wide-chain structures and various zipper-termination features occur within the subgrains. Many wide chains start from

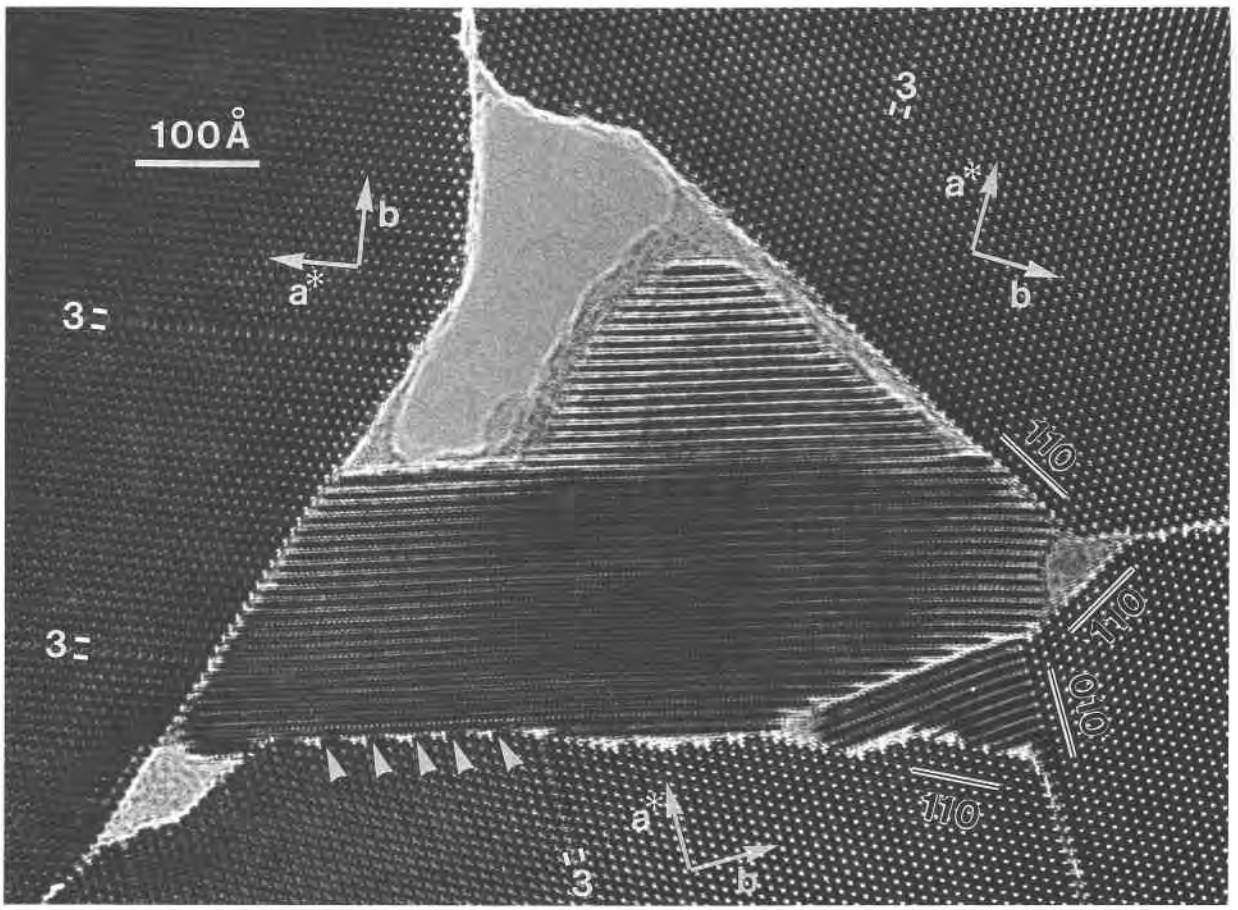

Fig. 6. Mica along grain boundaries between crocidolite crystals. Crocidolite (010) interfaces with mica are most abundant, and (110) interfaces also occur. Where crocidolite and mica have orientations that do not permit coherent (010) or (110) interfaces, serrated boundaries (indicated by arrows) develop.

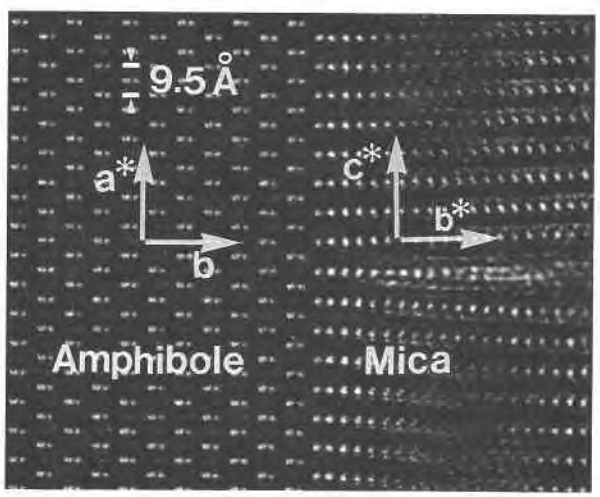

Fig. 7. HRTEM image of a coherent (010) interface between crocidolite and mica. The white spots of the mica at the interface are more closely spaced than elsewhere in the mica, suggesting that the structure at the interface differs slightly from that of the rest of the mica.

subgrain boundaries, and most terminate inside subgrains. The gaps between (010) boundaries of slightly rotated subgrains are filled with wide-chain materials whose chain widths change slightly to conform to the gaps caused by the rotations. The result is a wedgelike appearance of wide-chain pyriboles. Similar features were reported by Crawford (1980). Although most subgrains are irregular in shape, parts of subgrain boundaries parallel (010), (100), and (110). Figure 14 shows a crystal that contains a rich variety of defects. It is partly polygonized to several subgrains that are slightly misoriented with respect to one another; the numerous defects and intergrown wide-chain pyriboles define the outlines of misoriented domains.

Subgrain boundaries show various types of low-angle grain boundaries. In places, the I-beam units of amphibole are structurally continuous along **a*** across the low-angle grain boundaries despite the misorientation of the subgrains (Fig. 15). Elsewhere, well-defined grain boundaries do not occur between slightly misoriented subgrains (Fig. 16). There appears to be structural continuity between most parts of subgrains, but unusual contrast in the TEM images suggests that high strains may be asso-

ciated in such areas because of the misfits caused by misorientation.

Discussion

Polygonization in crocidolite

The shapes of subgrains are mainly defined by various planar defects and wide-chain pyriboles (Figs. 13–15), indicating that these features are closely related to the polygonization of crocidolite. Subgrain boundaries apparently formed by the propagation of (100) and (110) defects across which crystals are slightly rotated. Subgrains commonly show (100) and (110) boundaries (Figs. 13–15).

The areas around (100) and (110) defects contain Burgers vectors parallel to [100]. The areas containing dislocations have extra strain energy, and the (100) and (110) planar defects are apparently generated from such dislocations (e.g., Figs. 10 and 11). Wide-chain pyriboles commonly terminate incoherently at those defects (Figs. 11 and 12), resulting in lattice strain across the planar defects. The strain caused by incoherent termination also facilitated the crystal rotations across such defects.

Where rotations occur across several different (100) and (110) defects in the same crystal, some domain boundaries will be under tensile stress. The wedge-shaped gaps at (010) boundaries that are filled with wide-chain pyriboles apparently formed when crystals under tensile stress were separated across the (010) boundaries. The polygonization was completed when (100) and (110) defects and (010) boundaries grew over time, resulting in segregation into several subgrains with slight misorientations. The resulting subgrains are virtually free of strain and are presumably more stable than the initially strained parent crystal.

Fiber-formation mechanisms in crocidolite

Alario Franco et al. (1977) showed that fibrous crocidolite crystals are rotated with respect to each other, and Whittaker (1979) suggested that each fiber apparently nucleated separately and grew laterally until it contacted neighboring fibers. Walker and Zoltai (1979) suggested that amphibole asbestos was produced by spiral growth about a central screw dislocation, implying that fibrous crystals were produced during primary crystallization. Whittaker et al. (1981) inferred the presence of screw dislocations in amosite. However, Veblen (1980) found no evidence for screw dislocations in fibrous anthophyllite, and he suggested that spiral growth may not account for the elongation of amphibole asbestos. We also have seen no evidence of screw dislocations, although, as stated above, screw components parallel to [001] cannot be observed from [001] images.

Many fibrous crystals observed in the present study are rotated less than 10° with respect to adjacent crystals, and groups of fibers having similar orientations can be identified (Fig. 2). If each fiber originally crystallized separately, such preferred orientation would be improbable. However, if amphibole initially crystallized as large crystals and if they subsequently disaggregated into smaller elongated crystals without severe disruption of their general orientations, the fibers derived from a parent crystal would be expected to retain similar orientations. The possible derivation of fine fibers from larger crystals is also supported by textures showing small crystals having irregular shapes within or at the edges of large crystals (e.g., Fig. 3). Similar textural features were reported in TEM observation of fibrous anthophyllite (Veblen, 1980) and amosite (Cressey et al., 1982).

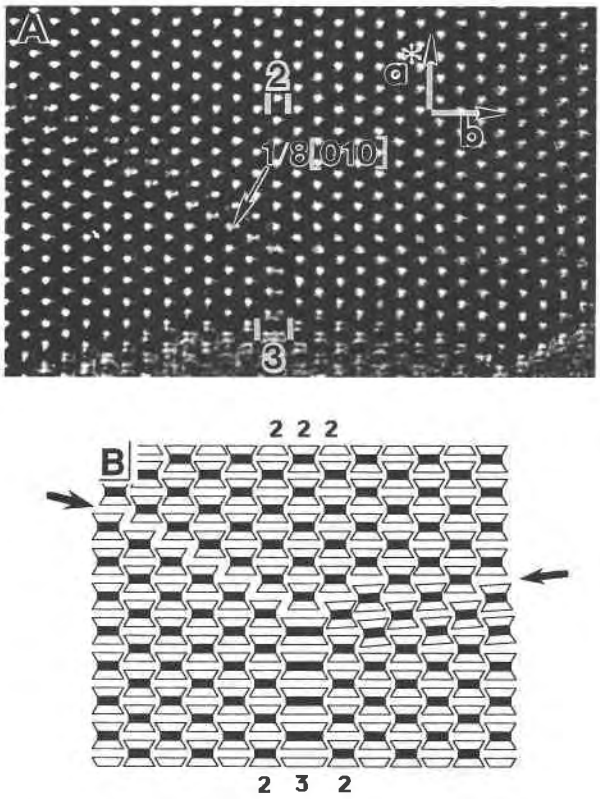

Fig. 8. (**A**) A triple chain (3) terminates incoherently to a double chain (2). Half of the chain-width misfit is compensated by an ⅛[010] displacive fault on one side of the zipper, and the other half is accommodated by slight distortions of I-beam units on the opposite side of the zipper. (**B**) A schematic model showing an ⅛[010] fault and I-beam distortion caused by the incoherent termination of the triple chain. The arrows point to the disrupted regions. In this and other figures, sighting along and across the defects at a low angle to the page will make it easier to see the discontinuities.

Geological stresses may have contributed to disaggregating polygonized crystals. Large asbestos deposits developed under stress-related structural conditions (Peacock, 1928; Trendall and Blockley, 1970). Dreyer and Robinson (1978) found that fiber development occurs where two sets of folds intersect to form domes or basins. If geologic stresses were exerted on iron formations that contained crystals that had already polygonized into subgrains, the partially coherent bonds between subgrains could readily be broken to produce fibrous crystals. Large

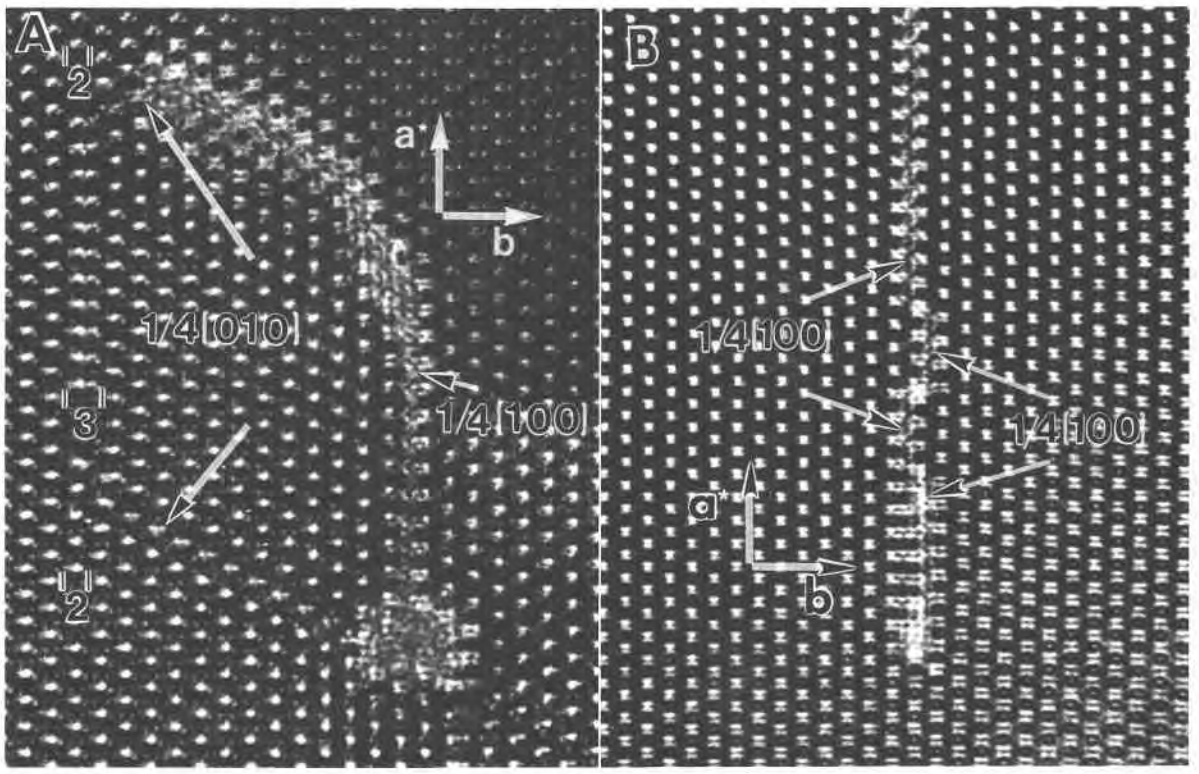

Fig. 9. (**A**) HRTEM image of a ¼[100] displacive fault. The terminating areas of the (010) slip plane are indistinct, presumably because of structural distortions at these areas. (**B**) Wide-chain pyriboles occur along a (010) plane that serves as a slip plane. Note that the ¼[100] marked in the images is an approximation and actually represents ¼[100] sin β.

crystals could have been disaggregated along the various structural defects to smaller crystals by the geologic stresses, even where complete subgrain boundaries had not developed. The breakage along subgrain boundaries and other defects would produce smaller crystals that would be misoriented by only a few degrees.

Polygonization of crocidolite is apparently critical for producing fibrous crystals. The present HRTEM study reveals that various structural defects are intimately associated with polygonization to smaller crystals. In particular, crocidolite may have crystallized with a high density of edge dislocations, and these dislocations then would have played an important role in polygonization and fiber formation. Such dislocations can serve as "seeds" for pla-

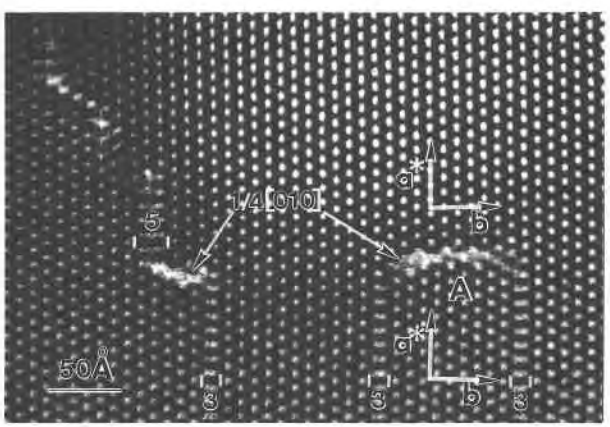

Fig. 10. Defects that are approximately parallel to (100). Slight misorientations occur across the defects, and ¼[010] displacive faults form as a result of incoherent zipper terminations.

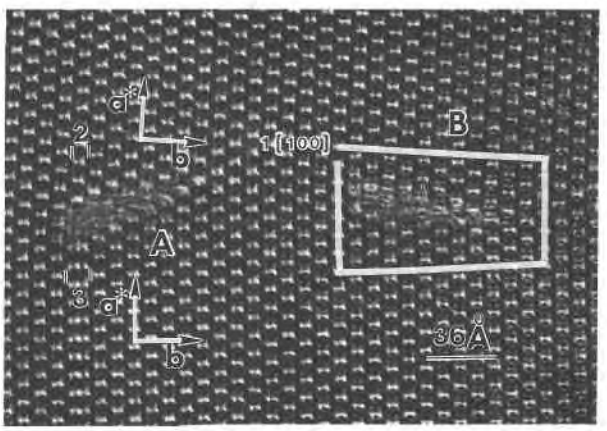

Fig. 11. A crystal showing (110) defects across which slight misorientations occur. A triple chain (3) terminates to a double chain (2) at the defect on the left side of the figure, but no zipper terminations occur on the right. The resulting 1[100] Burgers vector in the right-side defect indicates that an edge-dislocation component is present. Note that the 1[100] marked in the image is an approximation and actually represents 1[100] sin β.

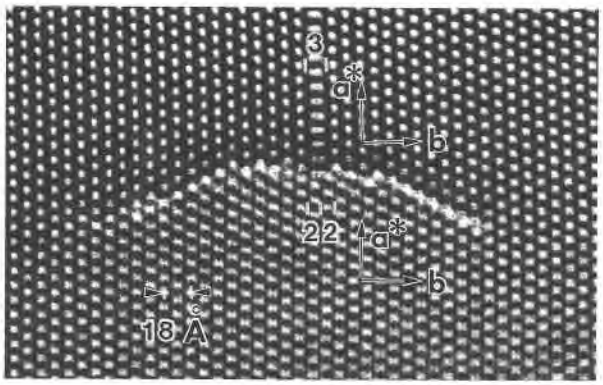

Fig. 12. The (110) and (100) defects are combined. A triple chain (3) changes to two double chains (22) at the defect, and slight rotation occurs across it.

nar defects that eventually take form as low-angle grain boundaries between subgrains.

TEM observation of Salton Sea samples by Yau et al. (1986) showed that amphiboles can grow as fine fibrous crystals, indicating that some fibrous crystals are primary. The occurrence of commercial asbestiform amphiboles in veins with the crystal fiber lengths perpendicular to the vein walls suggests that the fibrous morphology developed during the separation of the vein walls (Taber, 1916; Dreyer and Robinson, 1978; Veblen, 1980). However, the present TEM observations suggest that fibrous amphibole crystals can be polygonized into finer fibers by the growth of structural defects. Furthermore, it appears that some crocidolite fibers developed from nonasbestiform crystals by the polygonization process; stresses imposed on the iron formations presumably have assisted in the disaggregation of large crystals into fibrous forms.

Tensile strength of asbestos

The primary cause for the strong physical strength of asbestos has been attributed to the paucity of surface defects in asbestiform amphiboles relative to acicular amphiboles (Zoltai, 1979; Walker and Zoltai, 1979). However, no direct TEM evidence supporting systematic differences in surface defect densities between different amphiboles was found by Veblen (1980), who suggested that the physical differences between them may result from crystal size differences. If asbestiform and acicular amphiboles have the same dislocation densities, the smaller sizes of individual asbestiform fibers mean they will contain fewer dislocations that can then serve as sites for failure than do acicular fibers.

Many TEM studies show that almost all fibrous amphiboles are rich in structural defects (Chisholm, 1973;

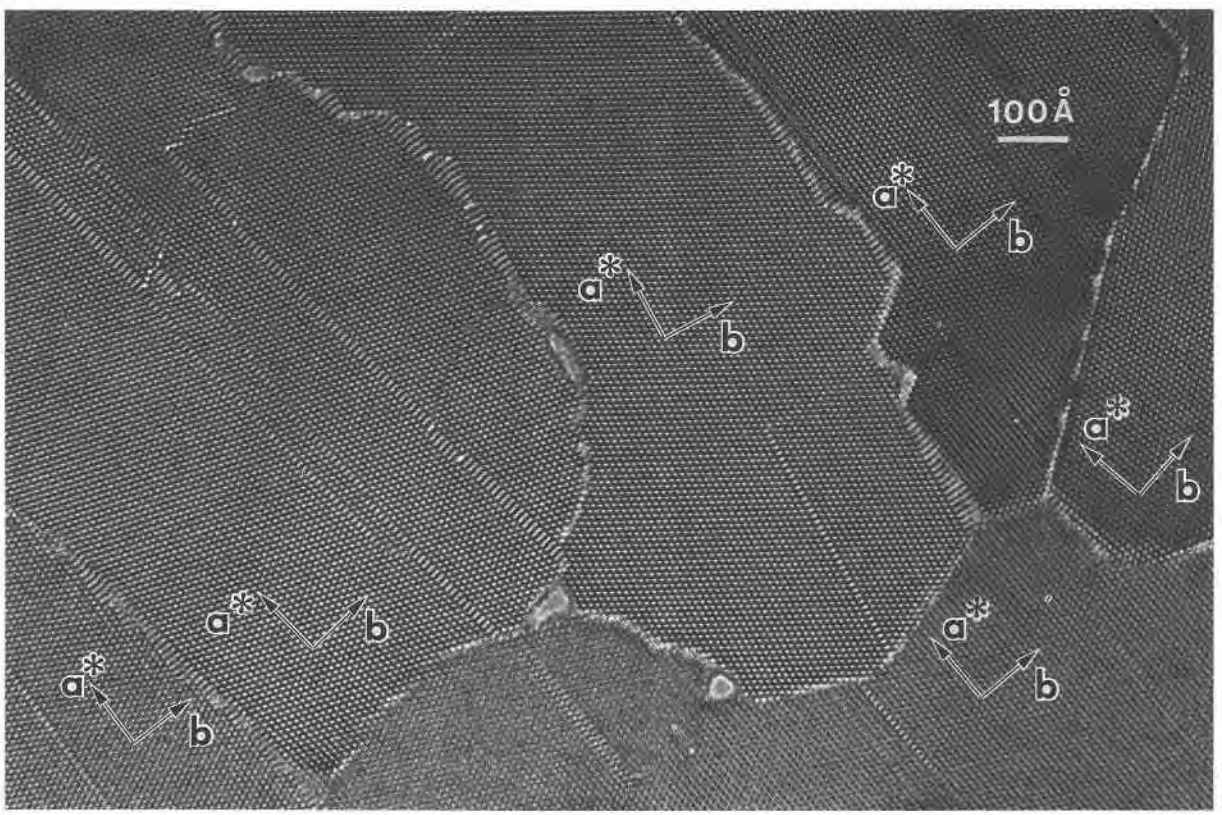

Fig. 13. A crystal that was polygonized to slightly rotated subgrains. Chain-width errors and zipper terminations are common within the subgrains. The (010) boundaries are relatively well defined, and the gaps between (010) boundaries of adjacent subgrains are filled by wedge-shaped masses of wide-chain biopyriboles. Boundaries having other orientations are not as well defined.

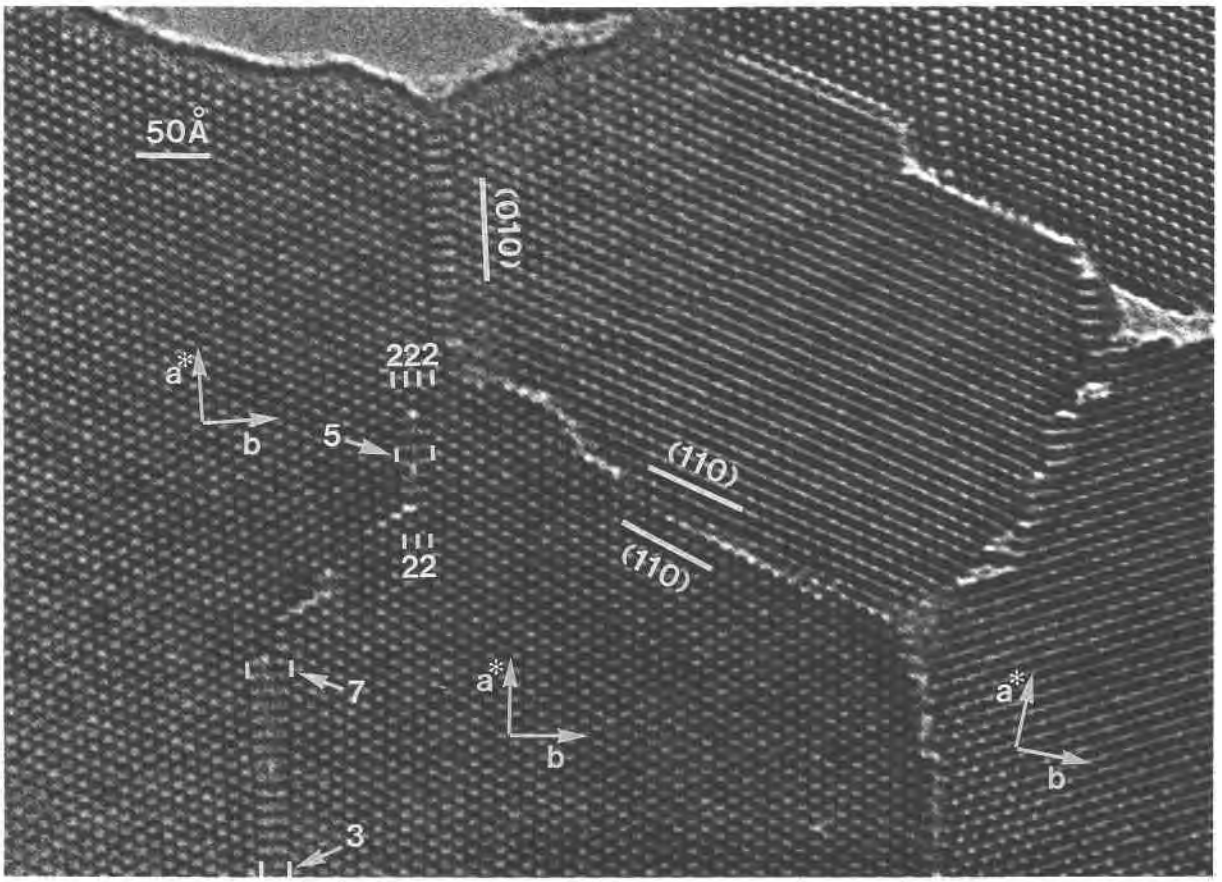

Fig. 14. A partly polygonized crystal. A small subgrain is formed by the wide chains along (010) and (110) defects. In addition, a variety of wide-chain pyriboles occur within the crystal.

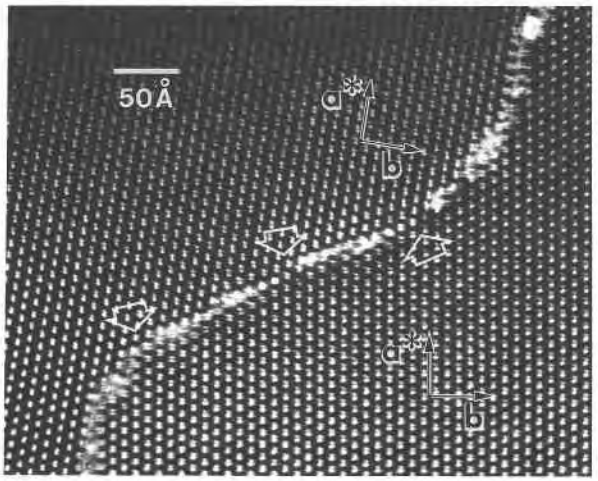

Fig. 15. A partly coherent low-angle grain boundary. The I-beam units are apparently continuous along **a*** across the boundary without much disruption (see the areas marked by arrows).

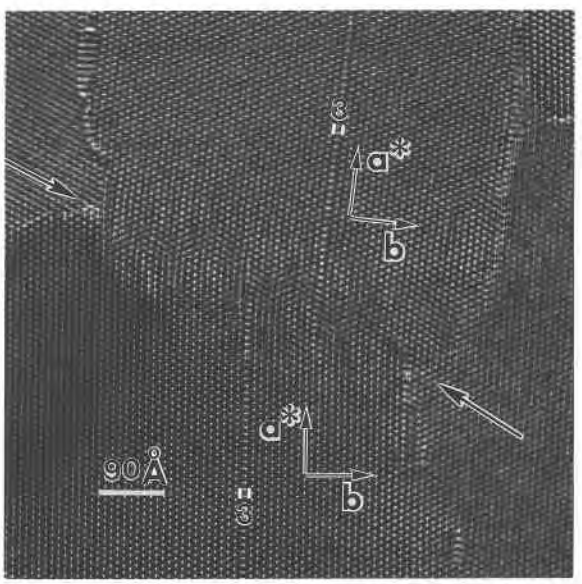

Fig. 16. A boundary between subgrains having slightly different orientations. A distinct, well-defined boundary does not occur here, and the boundary region is apparently highly strained. Triple chains in both subgrains are offset at the boundary (between the arrows).

Hutchison et al., 1975; Veblen et al., 1977; Veblen and Buseck, 1980; Veblen, 1980, 1981), and our data also support such observations. Fibrous amphiboles appear to contain higher densities of structural defects than nonfibrous ones, and therefore they may contain more abundant surface defects than massive amphiboles. The results of etching experiments by Walker (1981) indicate that the density of surface defects is lower in amphibole asbestos than in cleavage fragments. Instead, planar defects such as stacking faults and chain-width defects that are abundant in fibrous amphiboles seem to be important in increasing tensile strength (Chisholm, 1975). Cracks may propagate until they reach such defects and then proceed by slip parallel to the planar defects (Hodgson, 1979).

Various defects and polygonized subgrain boundaries observed in the present study are weakly bonded, and they can serve as walls mitigating brittle failure by providing sites for interplanar slip within a crystal. Grain boundaries are abundant in asbestiform amphiboles, and they can also impede the propagation of cracks caused by brittle failure, and they provide the sites for interplanar slip that results in high tensile strengths.

Conclusions

Crocidolite fibers are slightly rotated with respect to each other, and they show a wide range of diameters. Chain-width disorder and planar defects are common. The only observed sheet silicate is mica, and the absence of serpentine and chlorite minerals as hydration products is attributed to the Fe- and Na-rich composition of crocidolite.

Dislocations apparently developed during initial crystallization, and they may have served as seeds for the development of the (110) and (100) planar defects that are associated with crystal misorientations. Incoherent terminations of wide-chain pyriboles also apparently facilitated the development of such planar defects by causing lattice strain. Crocidolite grains tend to polygonize to smaller crystals; the propagation of defects associated with crystal misorientation results in subgrains that show partially coherent low-angle grain boundaries along (110), (100), and (010).

A variety of structural defects and polygonization features combined with the orientations of fibrous crystals strongly indicate that some fibers developed from larger crystals. Stress-related geologic environments presumably assisted in the separation of amphiboles into smaller, independent fibrous crystals by breaking the bonds across semicoherent, low-angle grain boundaries between subgrains and other planar defects. Subgrain boundaries and other defects are also presumably responsible for the high tensile strength of asbestiform amphiboles.

Acknowledgments

We are grateful to R.C. Morris and the CSIRO Division of Minerals and Geochemistry for providing samples and data. We thank C.M. Lesher for drawing our attention to the specimens and J.C. Clark for help with electron microprobe analysis. Helpful reviews were provided by S. Turner and T.C. McCormick. Electron microscopy was performed at the Facility for High Resolution Electron Microscopy at Arizona State University. The ASU HREM facility is supported by NSF and ASU, and this study was supported by NSF grant EAR-870529. The electron microprobe was obtained through NSF grant EAR-848167.

References cited

Ahn, J.H., Burt, D.M., and Buseck, P.R. (1988) Alteration of andalusite to sheet silicates in a pegmatite. American Mineralogist, 73, 559–567.

Alario Franco, M., Hutchison, J.L., Jefferson, D.A., and Thomas, J.M. (1977) Structural imperfection and morphology of crocidolite (blue asbestos). Nature, 266, 520–521.

Chisholm, J.E. (1973) Planar defects in fibrous amphiboles. Journal of Material Science, 8, 475–483.

——— (1975) Crystallographic shear in silicate structures. Surface and defect properties of solids, chapter 5. Chemical Society of London, London, England.

Cilliers, J.J. le R., and Genis, J.H. (1964) Crocidolite asbestos in the Cape Province. In S.H. Haugton, Ed., The geology of some ore deposits in southern Africa, vol. II, p. 579–591. Geological Society of South Africa, Johannesburg, South Africa.

Crawford, D. (1980) Electron microscopy applied to studies of the biological significance of defects in crocidolite asbestos. Journal of Microscopy, 120, 181–192.

Cressey, B.A., Whittaker, E.J.W., and Hutchison, J.L. (1982) Morphology and alteration of asbestiform grunerite and anthophyllite. Mineralogical Magazine, 46, 77–87.

Dreyer, C.J.B., and Robinson, H.A. (1978) The occurrence and exploitation of amphibole asbestos in South Africa. Preprint no. 78-H-64, Society of Mining Engineers, p. 1–21. AIME, Salt Lake City, Utah.

Ewers, W.E., and Morris, R.C. (1980) Chemical and mineralogical data from the uppermost section of the upper BIF member of the Marra Mamba Iron Formation. CSIRO, Institute of Earth Resources, Division of Mineralogy, Report no. FP 23, 15 p.

Hodgson, A.A. (1979) Chemistry and physics of asbestos. In L. Michaels and S.S. Chissick, Eds., Asbestos, vol. 1: Properties, applications, and hazards, p. 67–114. Wiley, New York.

Hutchison, J.L., Irusteta, M.C., and Whittaker, E.J.W. (1975) High-resolution electron microscopy and diffraction studies of fibrous amphiboles. Acta Crystallographica, A31, 794–801.

Iijima, S., and Buseck, P.R. (1978) Experimental study of disordered mica structures by high-resolution electron microscopy. Acta Crystallographica, A34, 709–719.

Klein, C., Jr., and Gole, M.J. (1981) Mineralogy and petrology of parts of the Marra Mamba Iron Formation, Hamersley Basin, Western Australia. American Mineralogist, 66, 507–525.

Mossman, B.T., Bignon, J., Corn, M., Seaton, A., and Gee, J.B.L. (1990a) Asbestos: Scientific developments and implications for public policy. Science, 247, 294–301.

——— (1990b) Asbestos, carcinogenicity, and public policy (letters and replies). Science, 248, 795–801.

Papike, J.J., Cameron, K.L., and Baldwin, K. (1974) Amphiboles and pyroxenes: Characterization of other than quadrilateral components and estimates of ferric iron from microprobe data. Geological Society of America Abstracts with Programs, 6, 1053–1054.

Peacock, M.A. (1928) The nature and origin of the amphibole asbestos of South Africa. American Mineralogist, 13, 241–285.

Ross, M. (1981) The geologic occurrences and health hazards of amphibole and serpentine asbestos. In Mineralogical Society of America Reviews in Mineralogy, 9A, 279–323.

Skinner, H.C.W., Ross, M., and Frondel, C. (1988) Asbestos and other fibrous materials. Oxford University Press, New York.

Smith, D.J., Barry, J.C., Bursill, L.A., Petford, A.K., and Wheatley, J.C. (1986) Atomic resolution imaging of crystalline defects and surfaces. JEOL News, 24E, 2–6.

Taber, S. (1916) The origin of veins of the asbestiform minerals. Proceedings of National Academy of Sciences, 2, 659–664.

Trendall, A.F., and Blockley, J.G. (1970) The iron formations of the

Precambrian Hamersley Group, Western Australia. Geological Survey of Western Australia Bulletin, 119, 366 p.

Veblen, D.R. (1980) Anthophyllite asbestos: Microstructures, intergrown sheet silicates, and mechanisms of fiber formation. American Mineralogist, 65, 1075–1086.

——— (1981) Non-classical pyriboles and polysomatic reactions in biopyriboles. In Mineralogical Society of America Reviews in Mineralogy, 9A, 189–236.

Veblen, D.R., and Buseck, P.R. (1979a) Chain-width order and disorder in biopyriboles. American Mineralogist, 64, 687–700.

——— (1979b) Serpentine minerals: Intergrowths and new combination structures. Science, 206, 1398–1400.

——— (1980) Microstructures and reaction mechanisms in biopyriboles. American Mineralogist, 65, 599–623.

——— (1981) Hydrous pyriboles and sheet silicates in pyroxenes and uralites: Intergrowth microstructures and reaction mechanisms. American Mineralogist, 66, 1107–1134.

Veblen, D.R., Buseck, P.R., and Burnham, C.W. (1977) Asbestiform chain silicates: New minerals and structural groups. Science, 198, 359–365.

Walker, J.S. (1981) Asbestos and the asbestiform minerals. M.S. thesis, University of Minnesota, Minneapolis, Minnesota.

Walker, J.S., and Zoltai, T. (1979) A comparison of asbestiform fibers with synthetic crystals known as "whiskers." Annals of New York Academy of Sciences, 330, 687–704.

Whittaker, E.J.W. (1979) Mineralogy, chemistry, and crystallography of amphibole asbestos. In R.L. Ledoux, Ed., Short course in mineralogical techniques of asbestos determination, p. 1–34. Mineralogical Association of Canada, Toronto.

Whittaker, E.J.W., Cressey, B.A., and Hutchison, J.L. (1981) Terminations of multiple-chain lamellae in grunerite asbestos. Mineralogical Magazine, 44, 27–35.

Yau, Y.-C., Peacor, D.R., and Essene, E.J. (1986) Occurrence of wide-chain calcium pyriboles as primary crystals in the Salton Sea Geothermal Field, California, USA. Contributions to Mineralogy and Petrology, 94, 127–134.

Zoltai, T. (1979) Asbestiform and acicular mineral fragments. Annals of the New York Academy of Sciences, 330, 621–642.

Manuscript received September 18, 1990
Manuscript accepted May 23, 1991